Supporting Information

DrFLINC Contextualizes Super-resolution Activity Imaging

Wei Lin[†,‖], Gary C. H. Mo[†,#,‖], Sohum Mehta[†], and Jin Zhang[†,¶,§,*]

[†]Department of Pharmacology, University of California, San Diego, La Jolla, CA 92093, United States

[¶]Department of Bioengineering, University of California, San Diego, La Jolla, CA 92093, United States

[§]Department of Chemistry and Biochemistry, University of California, San Diego, La Jolla, CA 92093, United States

[#]Present address: Department of Pharmacology and Regenerative Medicine, University of Illinois at Chicago, Chicago, IL 60612, United States

[*]Email: jzhang32@ucsd.edu

[‖]W.L. and G.C.H.M. contributed equally to this work

Contents

Figure S1;
Figure S2;
Figure S3;
Figure S4;
Figure S5;
Figure S6;
Figure S7;
Figure S8;
Figure S9;
Figure S10;
Methods
References

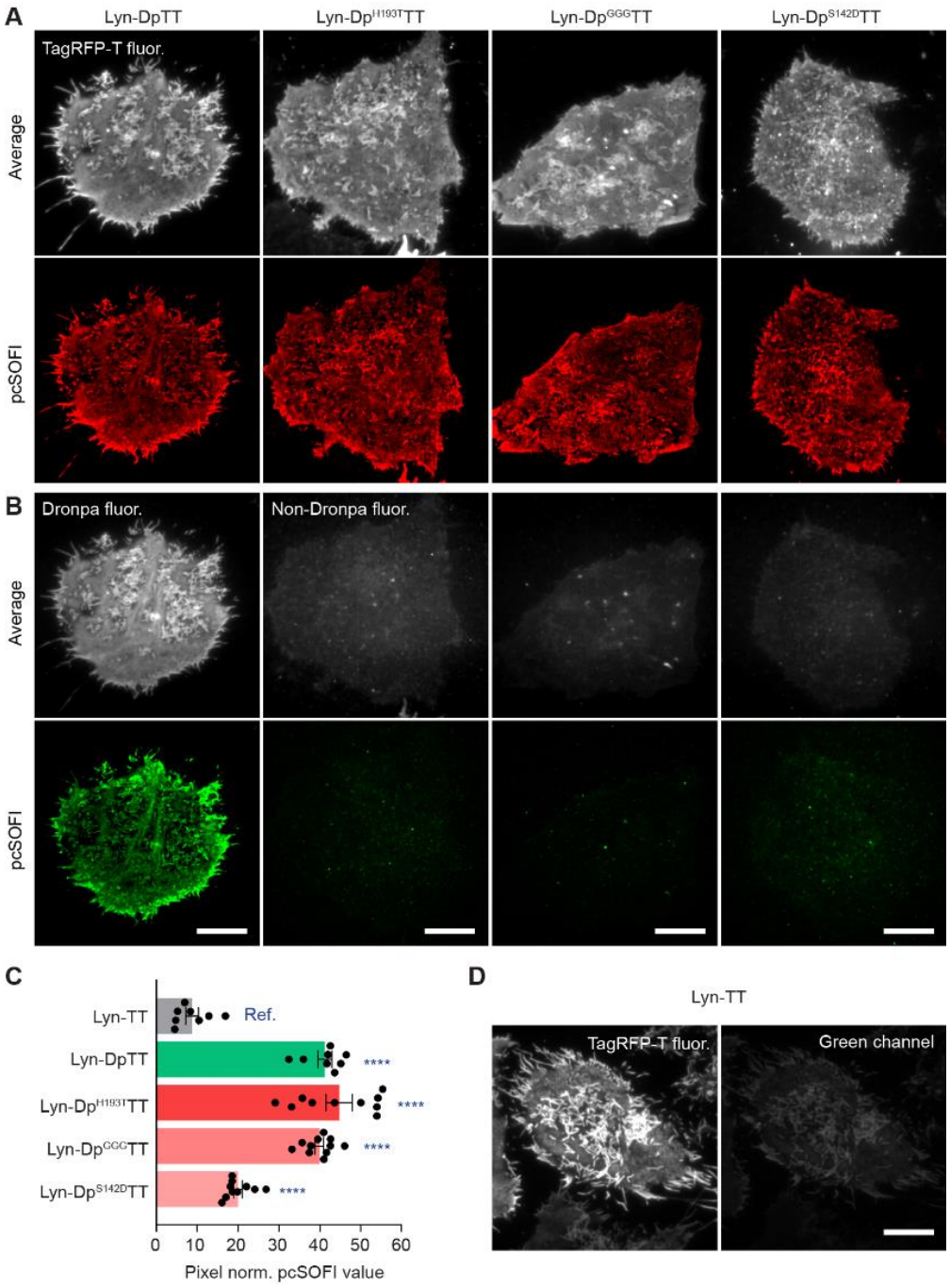

Figure S1. Characterization of DpTT, Dp^{H193T}TT, Dp^{GGG}TT and Dp^{S142D}TT. (A-B) Average fluorescence and 2nd order pcSOFI images of Lyn-DpTT, Lyn-Dp^{H193T}TT, Lyn-Dp^{GGG}TT and Lyn-Dp^{S142D}TT illuminated using 561-nm (A) and 488-nm (B) lasers. Images correspond to Figure 1B. Scale bars are 10 μm. (C) Comparison of TT only, DpTT, Dp^{H193T}TT, Dp^{GGG}TT and Dp^{S142D}TT suggests that Dronpa mutants can effectively induce FLINC except for S142D. Lyn-TT (n=8), Lyn-DpTT (n=8), Lyn-Dp^{H193T}TT (n=10), Lyn-Dp^{GGG}TT (n=11) and Lyn-Dp^{S142D}TT (n=10). The error bars represent mean ± s.e.m. (D) Average fluorescence of Lyn-TagRFP-T illuminated using 561-nm and 488-nm lasers. TagRFP-T

alone exhibits weak fluorescence in the green channel, suggesting that the weak green fluorescence observed in B is likely from TagRFP-T in the fusion constructs. Scale bars are 10 μm.

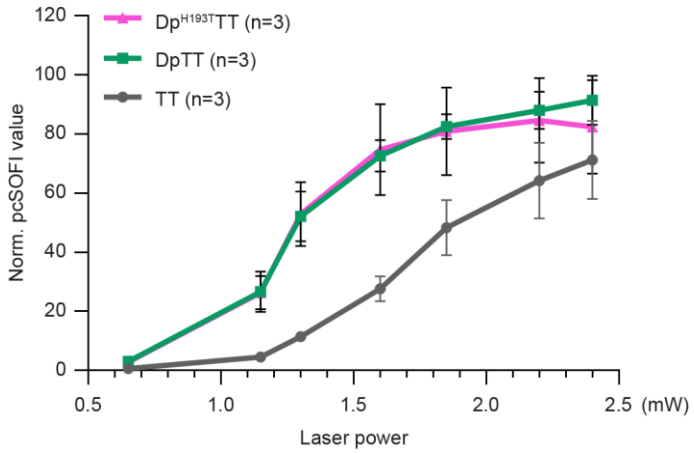

Figure S2. Excitation intensity modulates the fluorescence fluctuations of TagRFP-T alone or when fused with Dronpa variants. A 4-5 fold higher normalized pcSOFI signal compared to TagRFP-T alone was obtained with TagRFP-T fused to either WT or mutant Dronpa under 561-nm laser excitation at 1.3 mW. TT, DpTT, and Dp^{H193T}TT. The error bars represent mean ± s.e.m.

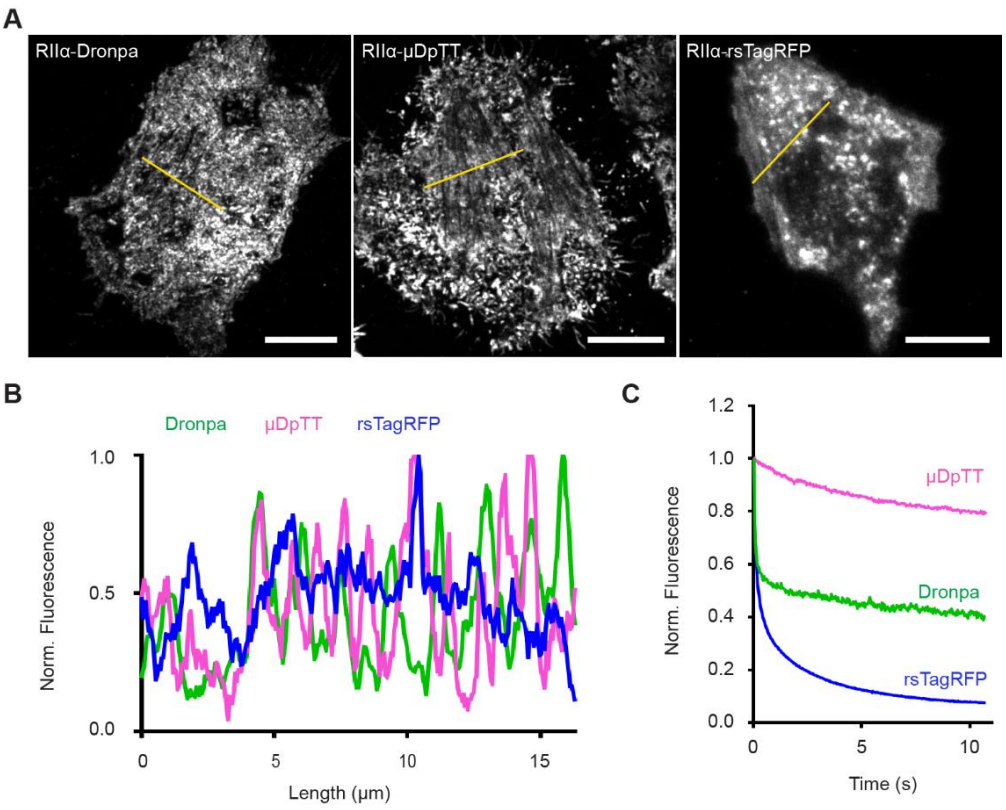

Figure S3. Comparison of Dronpa, μDpTT and rsTagRFP performances in pcSOFI imaging. (A) Comparison of 2nd order pcSOFI results for Dronpa-, μDpTT- and rsTagRFP-labeled PKA RIIα subunit in HeLa cells. Scale bars are 10 μm. (B) Line profiles of the pcSOFI images in (A) clearly show high signal amplitude and low background for Dronpa and μDpTT, but not rsTagRFP. (C) Average fluorescence time course of three RSFP-labeled cells shown in (A), showing the reduced switching contrast and more-pronounced bleaching for rsTagRFP.

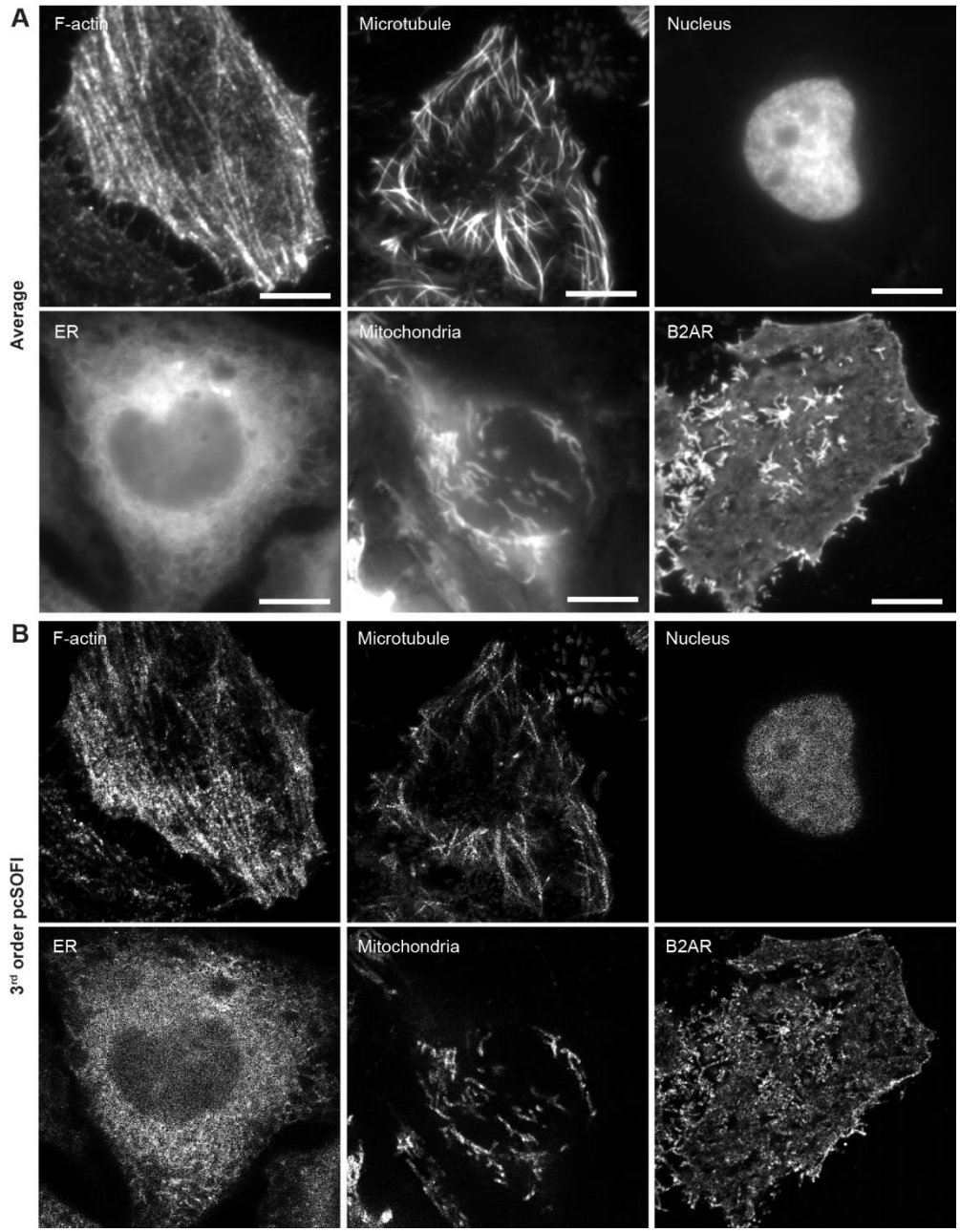

Figure S4. 3rd order pcSOFI images of μDpTT fusions. (A) Average fluorescence and (B) 3rd order pcSOFI images of Lifeact-μDpTT (F-actin), Tau-μDpTT (microtubule), H2B-μDpTT (nucleus), CYP450-μDpTT (ER), DAKAP1-μDpTT (mitochondria), and B2AR-μDpTT in HeLa cells illuminated with a 561-nm laser. Images correspond to Figure 2A. Scale bars are 10 μm.

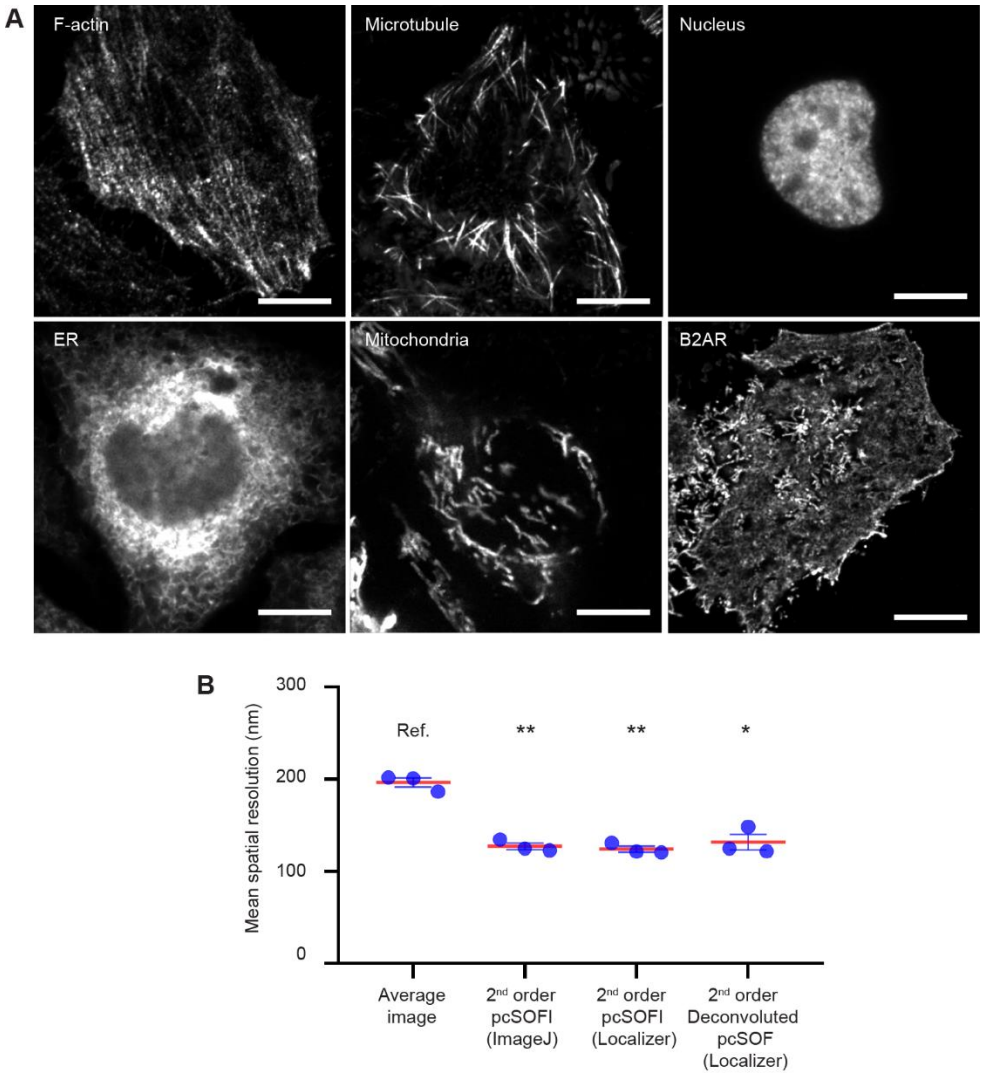

Figure S5. 2nd order pcSOFI images of µDpTT fusions with and without deconvolution. (A) 2nd order deconvoluted pcSOFI images of Lifeact-µDpTT (F-actin), Tau-µDpTT (microtubule), H2B-µDpTT (nucleus), CYP450-µDpTT (ER), DAKAP1-µDpTT (mitochondria), and B2AR-µDpTT in HeLa cells. Images correspond to Figure 2A. Scale bars are 10 µm. (B) Quantitative resolution estimation using Fourier ring correlation (FRC) analysis. Three replicates of Lifeact-µDpTT average images or 2nd order pcSOSI images calculated by ImageJ or Localizer with or without deconvolution are analyzed using the NanoJ-SQUIRREL ImageJ plug-in. The error bars represent mean ± s.e.m. The "Average" images generated by pcSOFI, while still diffraction limited, have resolution exceeding that of epifluorescence images.

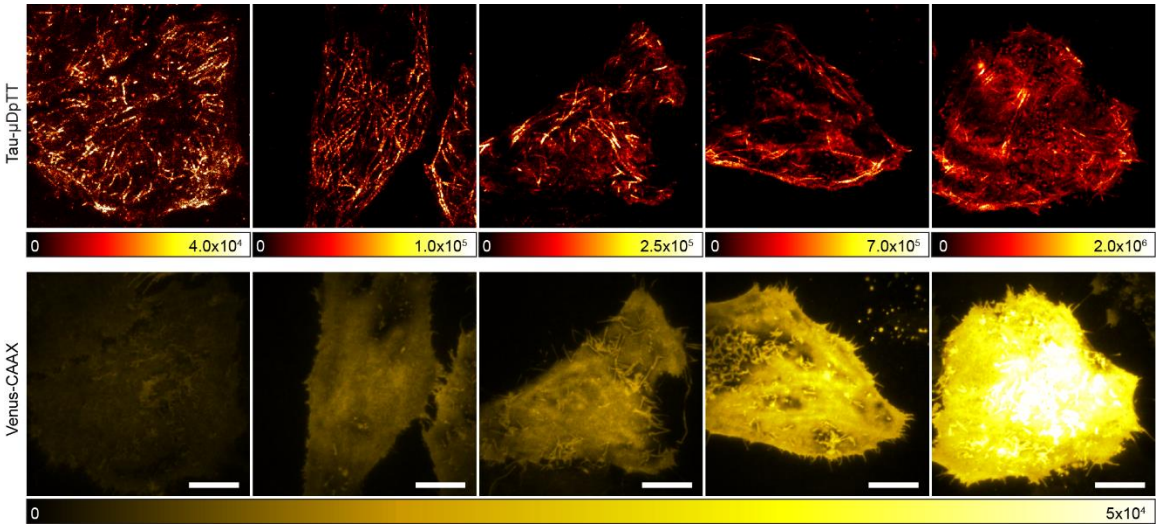

Fig. S6. Cells expressing different levels of tau-μDpTT are generally suitable for 2nd order pcSOFI. Expression level is estimated by P2A linked Venus-CAAX. The top panel showcases the representative pcSOFI images with appropriate contrast indicating that DrFLINC enables to generate high quality structural images of targets at different expression levels. The bottom panel shows the corresponding TIRF images of membrane targeted Venus with the same contrast indicating the different expression levels of the target protein. Scale bars are 10 μm.

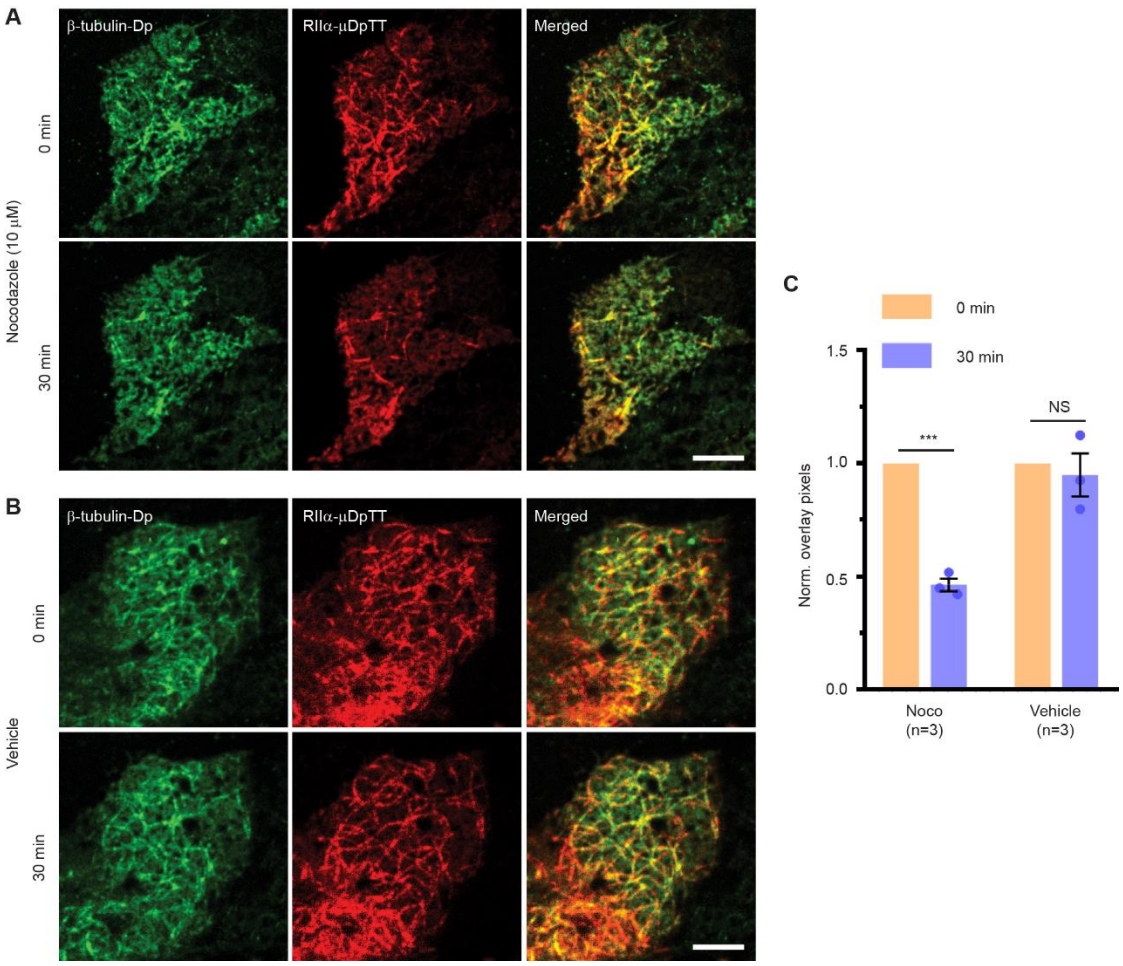

Figure S7. Dual-color pcSOFI images of dynamic changes as PKA RIIα localizations respond in tandem with microtubule depolymerization in MIN6 β cells. (A) Cells co-expressing RIIα-μDpTT and β-tubulin-Dp were treated with Nocodazole (Noco) for 30 min to disrupt microtubule polymerization. The fibrous RIIα structures dissociated along with microtubule depolymerization. (B) Vehicle-treated control cells retained abundant microtubule fibers with strong RIIα co-localization. Scale bars are 10 μm. (C) Quantification of RIIα-μDpTT and β-tubulin-Dp overlay pixels indicated that 54% of fibrous RIIα structures dissociated along with microtubule depolymerization, suggesting that RIIα indeed localizes on microtubules in MIN6 β cells. The error bars represent mean ± s.e.m.

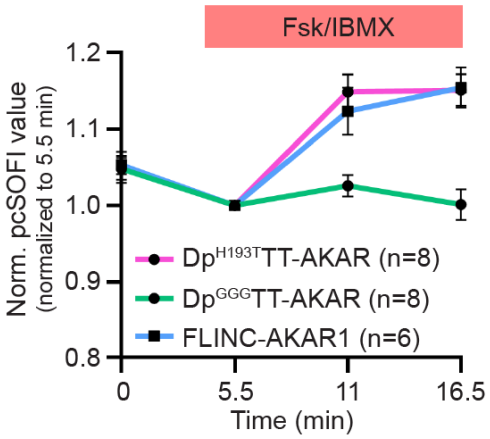

Figure S8. DrFLINC-AKAR PKA stimulation response using distinct Dronpa mutants. Average traces showing the mean normalized pcSOFI response time course from live HeLa cells expressing DrFLINC (Dp^{H193T}TT-AKAR), Dp^{GGG}TT-AKAR, and FLINC-AKAR1 after PKA stimulation. The error bars represent mean ± s.e.m.

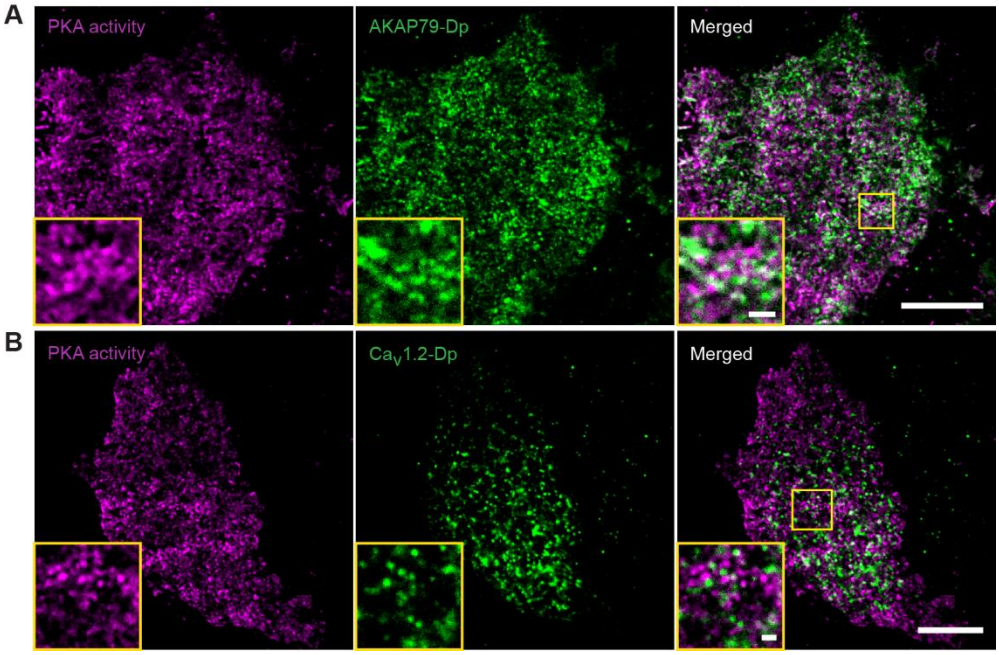

Figure S9. Dual-color pcSOFI imaging of basal PKA activity with different signaling components. (A) Co-imaging of PKA activity with AKAP79 in HeLa cells; (B) co-imaging of PKA activity with $Ca_v1.2$ in HEK293T cells. Zoomed-in views of the boxed regions are shown, where white color indicates colocalization. Scale bars are 10 μm (Insets: 1 μm).

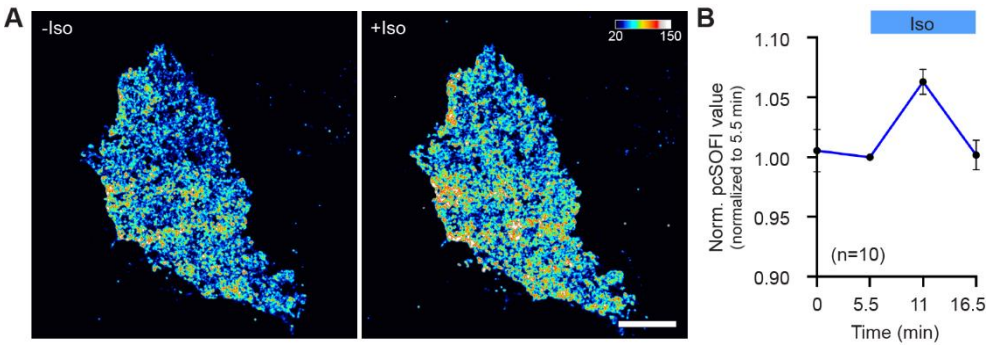

Figure S10. β-adrenergic stimulated response of DrFLINC-AKAR. (A) DrFLINC-AKAR super-resolution images clearly resolve the response to isoproterenol (Iso) stimulation (1 μM), and detailed spatial information on membrane PKA activity emerges. Color scales are identical. Scale bars are 10 μm. (B) Average trace showing the mean normalized pcSOFI response from live HEK293T cells expressing DrFLINC-AKAR after Iso stimulation. The error bars represent mean ± s.e.m.

Methods

Construct generation. Dronpa-DEVD-TagRFP-T (DpTT) and FLINC-AKAR1 generated in the previous work[1] were used as templates for mutant DpTTs and DrFLINC-AKAR cloning. All site-directed mutagenesis was performed according to a published protocol[2] with the primers for mutations on Dronpa, including 5'-ACT ATC ACT TTG TGG ACA CAC ACA TTG AGA TTA AAA GC-3' (H193T), 5'-ATC TTG ACA ACT GTG TTC GGA GGA GGA AAC AGG GTA TTC GCC AAA-3' (GGG) and 5'-ACT GTG AAA TGG GAG CCA GCC ACT GAG AAA TTG TAT G-3' (S142D), respectively. For mutant pairs targeted to plasma membrane, the N-terminal 11 amino acids from Lyn kinase (MGCIKSKRKDK) were fused at N-termini to generate Lyn-Dp^{H193T}TT, Lyn-Dp^{GGG}TT and Lyn-Dp^{S142D}TT. For Dp^{H193T}TT labeled proteins, the F-actin binding motif Lifeact (MGVADLIKKFESISKEE), the N-terminal 30 amino-acid leader sequence from DAKAP1 (MAIQLRSLFPLALPGMALLGWWWFFSRKK), the N-terminal 27 amino acids from CYP450 (MDPVVVLGLCLSCLLLLSLWKQSYGGG), the human β-2 adrenergic receptor (B2AR), and the PKA RIIα were cloned into pcDNA3-Dp^{H193T}TT plasmid to generate Lifeact-Dp^{H193T}TT, DAKAP-Dp^{H193T}TT, ER-Dp^{H193T}TT, B2AR-Dp^{H193T}TT and RIIα-Dp^{H193T}TT, respectively. The tau-Dp^{H193T}TT construct was generated by replacing Dronpa with Dp^{H193T}TT in Tau-Dronpa (Addgene #57286) plasmid. For Dronpa labeled proteins, the Lyn tag, Lifeact tag, PKA RIIα and AKAP79 were cloned at N-termini of Dronpa in pcDNA3 vector, while Dronpa-CAAX and Dronpa-$Ca_V1.2$ were generated by fusing the C-terminal targeting sequence from KRas (KKKKKSKTKCVIM) and the calcium channel $Ca_V1.2$ at C-termini of Dronpa, respectively. For tau-Dp^{H193T}TT-P2A-Venus-CAAX, the GSG-P2A-Venus-CAAX sequence was inserted between tau-Dp^{H193T}TT ORF and stop codon. β-tubulin-Dronpa (#57301) were ordered from Addgene. All constructs were verified by sequencing.

Cell culture and transfection. HeLa, HEK293T and MIN6 β cells were cultured in Dulbecco's modified Eagle medium and supplemented with 10% fetal bovine serum and 1% penicillin-streptomycin. All cells were maintained at 37 °C and 5% CO2 in a humidified incubator. For imaging, cells were plated onto sterile 35-mm glass-bottomed dishes and grown to ~50% confluence. Cells were then transfected using Lipofectamine 2000 (Invitrogen) and grown for an additional 24 h (HeLa, HEK293T) or 48 h (MIN6) before imaging.

Imaging acquisition. All pcSOFI imaging was performed on a commercial Olympus IX83 microscope equipped with a cellTIRF-4Line system, a 150× NA 1.45 objective and an Andor IXON Ultra 888 electron-multiplying CCD camera. All the images of Dronpa labeled proteins were illuminated by a Coherent 488-nm laser with 2.4 mW power (at the objective) in total internal reflection fluorescence (TIRF) mode, and all the images of DrFLINC were performed by a Cell* 561-nm laser with 1.3 mW power (at the objective) in TIRF mode except for H2B-Dp^{H193T}TT in HILO mode, and mitochondria and ER labeled Dp^{H193T}TT in epifluorescence mode. For single-color pcSOFI, all TIRF images and time-lapse series were captured at 35-ms exposure time for 850 frames (~30-s duration). For dual-color imaging, sequential acquisition with 561-nm and 488-nm illumination at 35-ms exposure time was utilized and 300 frames (~10-s duration) were recorded for each color. For time course activity imaging, 5.5-min interval time including ~30-s total acquisition and 5-min fluorescence recovery was used. Plasma membrane targeted Venus in Figure S4 were illuminated by a lower 488-nm laser power and acquired at 100-ms exposure time with low digital gain value of camera.

Data processing. pcSOFI calculations were performed using a custom ImageJ plug-in that implements the previously reported[3] Localizer pcSOFI calculations in Java and compiled using Eclipse IDE. The ImageJ plugin does not include 'deconvolution', an additional feature in Localizer pcSOFI where Gaussian PSF averaging can be optionally applied to further improve the super-resolution images. Otherwise, the second order correlation algorithms are the same as those previously reported, whereby cross-cumulant calculations were performed to generate 2nd or 3rd order cumulant values into a denser, enhanced grid containing virtual pixels[4]. The same normalization procedure is used as before[1]. Richardson-Lucy deconvolution of pcSOFI in Figure S5 was performed using Localizer with the following parameters: a Gaussian PSF with a standard deviation of 1.6 pixels and two iterations.

The spatial resolution of 2nd order SOFI images with or without deconvolution were estimated using Fiji and the plugin of the open source Nano-SQUIRREL published by Culley *et al*[5]. To create image pairs for FRC analysis, 850 TIRF image sequences were split into overlapping sub-sequences using the tool in the Nano-SQUIRREL package (even and odd frames). Then the custom ImageJ plug-in or Localizer were utilized to generate 2nd order sub-pcSOFI images. FRC maps were then created using appropriate blocks (20×20 blocks to average images and 50×50 blocks to pcSOFI) for good sampling of cell and background areas. The mean resolution was then determined by averaging FRC values of the different blocks within the cell area. Three cells from three independent experiments were analyzed for structural or activity imaging.

The thresholded Pearson's coefficients were calculated using Coloc 2 mode in ImageJ for Figure 2 and 4. The area of overlay fibers in Figure S7 was calculated by thresholding fluorescence intensity to highlight overlay regions and counting pixels using ImageJ. Statistical analyses were performed using GraphPad Prism 8 (GraphPad Software). All data shown are from at least three independent experiments. For Gaussian data, pairwise comparisons were performed

using Student's t-test or Welch's unequal variance t-test. *, $p<0.05$; **, $p<0.01$; ***, $p<0.001$; ****, $p<0.0001$; NS, not significant.

References

(1) Mo, G. C.; Ross, B.; Hertel, F.; Manna, P.; Yang, X.; Greenwald, E.; Booth, C.; Plummer, A. M.; Tenner, B.; Chen, Z., et al., Genetically encoded biosensors for visualizing live-cell biochemical activity at super-resolution. *Nat. Methods* **2017,** *14* (4), 427-434.
(2) Sawano, A.; Miyawaki, A., Directed evolution of green fluorescent protein by a new versatile PCR strategy for site-directed and semi-random mutagenesis. *Nucleic Acids Res.* **2000,** *28* (16), E78.
(3) Dedecker, P.; Mo, G. C.; Dertinger, T.; Zhang, J., Widely accessible method for superresolution fluorescence imaging of living systems. *Proc. Natl. Acad. Sci. U. S. A.* **2012,** *109* (27), 10909-10914.
(4) Dondelinger, R. F.; Kurdziel, J. C.; Capesius, C., Diagnosis of tumors originating from the bile ducts. *Bull. Soc. Sci. Med. Grand. Duche Luxemb.* **1988,** *125* (2), 5-14.
(5) Culley, S.; Albrecht, D.; Jacobs, C.; Pereira, P. M.; Leterrier, C.; Mercer, J.; Henriques, R., Quantitative mapping and minimization of super-resolution optical imaging artifacts. *Nat. Methods* **2018,** *15* (4), 263-266.